

Quantum Magic and Computational Complexity in the Neutrino Sector

Ivan Chernyshev ^{1,*}, Caroline E. P. Robin ^{2,3,†} and Martin J. Savage ^{1,‡}

¹*InQubator for Quantum Simulation (IQUS), Department of Physics,
University of Washington, Seattle, WA 98195, USA.*

²*Fakultät für Physik, Universität Bielefeld, D-33615, Bielefeld, Germany*

³*GSI Helmholtzzentrum für Schwerionenforschung, Planckstraße 1, 64291 Darmstadt, Germany*

(Dated: November 8, 2024)

We consider the quantum magic in systems of dense neutrinos undergoing coherent flavor transformations, relevant for supernova and neutron-star binary mergers. Mapping the three-flavor-neutrino system to qutrits, the evolution of quantum magic is explored in the single scattering angle limit for a selection of initial tensor-product pure states for $N_\nu \leq 8$ neutrinos. For $|\nu_e\rangle^{\otimes N_\nu}$ initial states, the magic, as measured by the $\alpha = 2$ stabilizer Renyi entropy \mathcal{M}_2 , is found to decrease with radial distance from the neutrino sphere, reaching a value that lies below the maximum for tensor-product qutrit states. Further, the asymptotic magic per neutrino, \mathcal{M}_2/N_ν , decreases with increasing N_ν . In contrast, the magic evolving from states containing all three flavors reaches values only possible with entanglement, with the asymptotic \mathcal{M}_2/N_ν increasing with N_ν . These results highlight the connection between the complexity in simulating quantum physical systems and the parameters of the Standard Model.

To optimize the impact of quantum computers in simulating key aspects of fundamental physics, it is essential to understand the required balance among quantum and classical computing resources to address specific observables. As advances in quantum simulations feed back to improve classical simulations, this balance changes with time, and guidance from the target physical systems must be folded in with each new advance. Robust simulations of neutrinos produced during supernova and during neutron-star binary mergers are important, e.g., Refs. [1–18], not only for their evolution and for the predictions of the chemical elements in such processes, but also for probing the properties and interactions of neutrinos themselves and potentially discovering new physics, e.g., Ref. [19]. As part of the integration of the neutrino processes that take place during a supernova into simulations, a much better understanding of the quantum complexity of coherent flavor transformations is essential.

During core-collapse supernova (CCSN), the neutrino density becomes sufficiently high that self-interactions play an essential role in the evolution of lepton flavor. There have been numerous studies performed to describe the impact of the $\sim 10^{58}$ neutrinos that are produced in such events. The range of mass-scales involved, and the interaction processes that take place, present a significant challenge to accurately describing this evolution. The mean-field and many-body approaches for the dynamics continues to provide a firm foundation, under-

pinning much of what is known about these systems, e.g., Refs. [20–29]. However, advances in quantum information are providing motivation and techniques to consider aspects of these systems beyond the currently employed approximations [30–44]. These nascent explorations, that include the low-energy effective Hamiltonian from the Standard Model mapped to all-to-all connected spin models, have examined the evolution of the neutrino flavors, their entanglement entropy, multi-partite entanglement using n -tangles, and more. Typically these have been performed using an effective two-neutrino system, and extensions to include three flavors are now beginning [45–49]. The entanglement between multiple neutrinos exceeds that of systems of Bell pairs, and hence is fundamentally multi-partite in nature [38, 41]. Simulations of modest-sized systems of neutrinos have been performed using superconducting-qubit and trapped-ion qubit quantum computers [38, 50–54]. Further, classical simulations [47] and preparations for quantum simulations using qutrits have also been recently performed [49]. Simulating neutrino environments of interest requires working with mixed states, and as such, these early investigations are important for guiding development toward more robust simulations.

The Gottesman-Knill theorem [55] and the work of Aaronson and Gottesman [56] make clear that entanglement is a necessary but not sufficient condition for the preparation of a given state to require a quantum computer. Significant quantum magic (non-stabilizerness) along with large-scale entanglement is the requisite for the need for quantum computation. Stabilizer states can be efficiently prepared using a classical gate set of the Hadamard-gate, H, the phase-gate, S, and the CNOT-gate [55, 57] (App. A). By construction, stabilizer states

* ivanc3@uw.edu

† crobin@physik.uni-bielefeld.de

‡ mjs5@uw.edu; On leave from the Institute for Nuclear Theory.

have vanishing measures of magic. Thus, both magic and entanglement determine the computational complexity and quantum resource requirements for simulating physical systems. Including the T-gate to establish a universal quantum gate set, Gottesman-Knill-Aaronson [55, 56] showed that the exponential-scaling (with system size) of classical resource requirements is determined by the minimum number of T-gates (a similar argument exists for scaling with precision, e.g., Ref. [58]). A number of measures of magic have been developed, e.g., Refs. [59–64], and the stabilizer Rényi entropies (SREs) [65] and Bell magic [66] have been measured in quantum simulations of some systems [66–68], and are efficiently calculable in MPS [69–72]. The magic properties of physical many-body systems and quantum field theories are less known than their entanglement structures. Explorations in the Ising and Heisenberg models [67, 70, 73–75], lattice gauge models [76], quantum gravity [77], in nuclear and hypernuclear forces [78], and in the structure of nuclei [79] are in their earliest stages. Interestingly, it has recently been shown that the entanglement and magic in random quantum circuits doped with T-gates and measurements undergo phase transitions (between volume-law and area-law scaling) at different dopings [58, 75, 80–82].

To determine the measures of magic in a wavefunction, matrix elements of strings of Pauli operators, \hat{P} , are computed, $c_P(t) \equiv \langle \psi(t) | \hat{P} | \psi(t) \rangle$. For qutrits, the Pauli strings are constructed from tensor-products of the nine operators, $\hat{\Sigma}_i$ [83–85],

$$\hat{\Sigma}_i \in \{\hat{I}, \hat{X}, \hat{Z}, \hat{X}^2, \omega \hat{X} \hat{Z}, \hat{Z}^2, \omega^2 \hat{X} \hat{Z}^2, \hat{X}^2 \hat{Z}, \hat{X}^2 \hat{Z}^2\}, (1)$$

where

$$\hat{X}|j\rangle = |j+1\rangle, \quad \hat{Z}|j\rangle = \omega^j|j\rangle, \quad \omega = e^{i2\pi/3}, (2)$$

for $j = 0, 1, 2$. For stabilizer states of n_Q qutrits, $d = 3^{n_Q}$ of the d^2 Pauli strings give $c_P = 1, \omega$ or ω^2 , while the other $d^2 - d$ give $c_P = 0$ [86]. For an arbitrary quantum state, all d^2 values can be non-zero. As is the case for qubits, the deviation from stabilizerness defines the magic in a state [65], using

$$\Xi_P = |c_P|^2/d, \quad \sum_P \Xi_P = 1, (3)$$

where Ξ_P forms a probability distribution. Based on our previous studies [78, 79], we consider the $\alpha = 2$ stabilizer Rényi entropy (SRE),

$$\mathcal{M}_2 = -\log_2 d \sum_P \Xi_P^2, (4)$$

to explore the quantum magic in a neutrino wavefunction. This SRE has been shown to satisfy properties of a proper magic measure [70, 87]. For more details, see App. B.

In the case of three flavors of neutrinos, the charged-current eigenstates are related to the mass eigenstates

by the Pontecorvo–Maki–Nakagawa–Sakata (PMNS) matrix [88, 89],

$$\nu_F = U_{PMNS} \nu_M, (5)$$

where, $\nu_F = (\nu_e, \nu_\mu, \nu_\tau)^T$ and $\nu_M = (\nu_1, \nu_2, \nu_3)^T$. Neglecting Majorana phases, U_{PMNS} can be parameterized in terms of three angles, $\theta_{12}, \theta_{13}, \theta_{23}$ and one CP-violating phase δ . The experimental determinations of these angles in a commonly used parameterization of the matrix are taken from the Particle Data Group (PDG) [90], and reproduced in App. C.

In the basis of mass eigenstates, the one-body Hamiltonian for a neutrino of energy E , has the form,

$$\hat{H}_1 = \frac{1}{2E} \begin{pmatrix} 0 & 0 & 0 \\ 0 & \delta m_{21}^2 & 0 \\ 0 & 0 & \Delta m_{31}^2 \end{pmatrix} + \dots, (6)$$

where the ellipses denote terms proportional to the identity matrix or higher order in the neutrino-mass expansion of the kinetic energy. The difference in mass-squareds, Δm_{31}^2 can be related to the experimentally measured values, $\Delta m_{31}^2 = \Delta m_{32}^2 + \delta m_{21}^2$ [90].¹ An effective two-flavor reduction of the system is typically found by retaining θ_{12} and δm_{21}^2 and discarding the third eigenstate.

In the mass basis, each neutrino flavor has non-zero magic from the U_{PMNS} mixing matrix. In the case of single electron-flavored neutrino in the effective two-flavor system, its magic is computed to be $\mathcal{M}_2 = 0.195(23)$, which should be compared to a maximum value of 0.415 for relatively real states and 0.585 for complex states. For a three-flavor neutrino, the magic in the single neutrino is found to be $\mathcal{M}_2 = 0.891(14)$, which should be compared with a maximum possible value of 1. The presence of the third generation of neutrinos changes the magic in the single neutrino sector substantially. To reinforce this observation, it is helpful to consider the magic power [65, 78] of the single-neutrino evolution operator. The magic power of a unitary operator, which we denote by $\overline{\mathcal{M}}_2$, quantifies the average fluctuations in magic induced by the operator, based upon its action on stabilizer states $|\Phi_i\rangle$. By considering the set of time evolved states, under the evolution of the free-space one-body Hamiltonian in Eq. (6),

$$|\Phi_i\rangle(t) = \hat{U}_1(t)|\Phi_i\rangle = e^{-i\hat{H}_1 t}|\Phi_i\rangle, (7)$$

the magic power of $e^{-i\hat{H}_1 t}$ is shown in Fig. 1. There is a significant difference between the magic power of the free-space one-body evolution operator for three flavors compared with two.

¹ In this work, only the normal hierarchy of neutrino masses is considered.

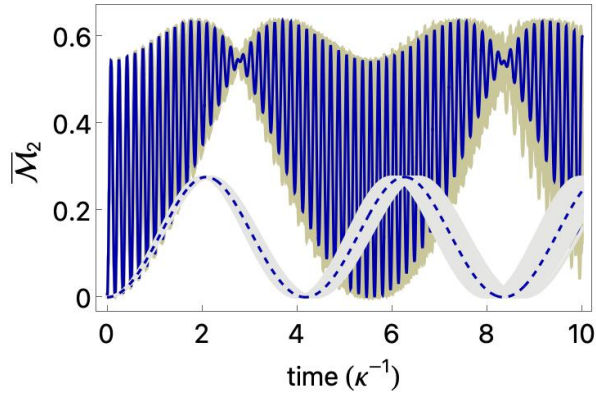


FIG. 1. The magic power, $\overline{\mathcal{M}}_2(\hat{U}_1)$, of the free-space one-body evolution operator for three flavors of neutrinos given in Eq. (7). The solid blue line shows the central value of the magic power, while the khaki region corresponds to the values of magic power from a sampling over the 68% confidence intervals of Δm_{32}^2 and δm_{21}^2 . The dashed-blue line and lighter shaded region correspond to the magic power of the evolution operator in the effective two-flavor system. Analytic expressions for $\overline{\mathcal{M}}_2(\hat{U}_1)$ are provided in App. D.

There are a number of models employed to expose essential elements of the coherent evolution of neutrinos in supernovae. We select one such model, that has been fruitfully used to study the evolution of entanglement, to illustrate the corresponding behavior of magic. The pairwise coherent forward interactions between neutrinos is captured by the low-energy position-dependent effective Hamiltonian [45, 91–99], combined with a (naively integrable) model-dependent neutrino density profile in the single-angle limit [47],

$$\hat{H}_2(r) = \mu(r) \sum_{a=1}^8 \hat{T}^a \otimes \hat{T}^a, \quad (8)$$

$$\mu(r) = \mu_0 \left(1 - \sqrt{1 - (R_\nu/r)^2} \right)^2,$$

where the \hat{T}^a are the generators of SU(3) transformations, and at the edge of the neutrino sphere, the model uses $\mu_0 = 3.62 \times 10^4$ MeV, $\kappa R_\nu = 32.2$, and $\kappa = 10^{-17}$ MeV. The time evolution of multi-neutrino systems is determined by integrating the action of the evolution operator on a given initial state. In this model, the radial location of the neutrinos is given by $r(t) = r_0 + t$, with $r_0 = 210.65/\kappa$ defining $t = 0$. Using a distribution of neutrino one-body energies below $E_0 = 10$ MeV, scaling as $E_n = E_0/n$, the time-dependent Hamiltonian and wavefunction evolution describing the coherent flavor evolution can be written as, assuming radial propagation,

$$\hat{H}(t) = \sum_n n \hat{H}_1^{(n)} + \sum_{n,n'} \hat{H}_2^{(n,n')}(t),$$

$$|\psi(t)\rangle = \hat{U}_2(t, 0) |\psi\rangle_0 = T \left[e^{-i \int_0^t dt' \hat{H}(t')} \right] |\psi\rangle_0, \quad (9)$$

where $\hat{H}_1^{(n)}$ is given in Eq. (6) acting on the n^{th} neutrino,

and $\hat{H}_2^{(n,n')}(t)$ corresponds to the two-body operator in Eq. (8) acting on the n^{th} and n'^{th} neutrinos.

In the two-neutrino sector, we consider initial conditions of a tensor-product pure-state of two electron-flavor neutrinos, $|\psi\rangle_0 = |\nu_e \nu_e\rangle$, and one electron with one muon flavor neutrinos, $|\nu_e \nu_\mu\rangle$, in the two-flavor and three-flavor frameworks. Evolving these states forward using $\hat{U}_2(t, 0)$ in Eq. (9) provides (pure-state) wavefunctions at some later time, from which the flavor composition, entanglement and magic are computed. Normalizing the magic in the wavefunction with respect to the maximum possible magic, gives the curves shown in Fig. 2. Fluctuations in

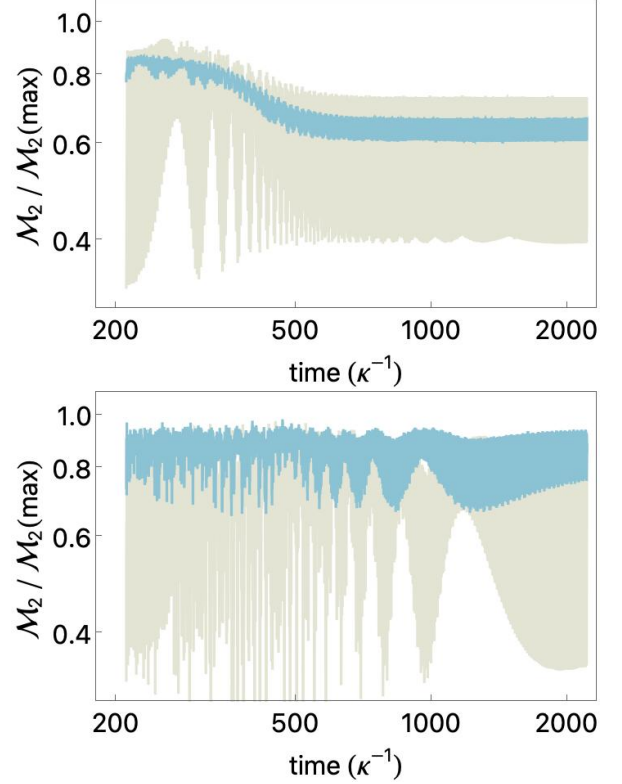


FIG. 2. The normalized magic in the two-flavor (lighter, cream) and three-flavor (darker, blue) neutrino wavefunctions as a function of time, starting in the pure tensor-product states $|\nu_e \nu_e\rangle$ (upper) and $|\nu_e \nu_\mu\rangle$ (lower). The \mathcal{M}_2 measure of magic, defined in Eq. (4), is normalized to its maximum value, $\mathcal{M}_2(\text{max}) = 1.19265$ for two flavors and $\mathcal{M}_2(\text{max}) = 2.23379$ for three flavors.

magic in the three-flavor system are significantly smaller than in the two-flavor system, but are consistent with each other. Both systems have stabilized with regard to their overall behavior for $\kappa t \gtrsim 600$, for which the maximum values of magic are 0.871 (two flavors) and 1.491 (three flavors). Interestingly, the magic in the $|\nu_e \nu_e\rangle$ systems decrease (on average) as the neutrinos move outward, while the magic in the $|\nu_e \nu_\mu\rangle$ systems do not show this trend.

Generalizing the analysis to the evolution of multi-neutrino systems is straightforward. An initial tensor-

product state of selected three-flavor structure is evolved forward in time using the evolution operator in Eq. (9). For a system of N_ν neutrinos, the magic is computed by evaluating forward matrix elements $c_P(t)$, defined above. The evolution of \mathcal{M}_2 as a function of time, computed using Eq. (4), is observed to stabilize after $\kappa t \gtrsim 800$, and its asymptotic value is determined by averaging over a time interval at much later times. The time depen-

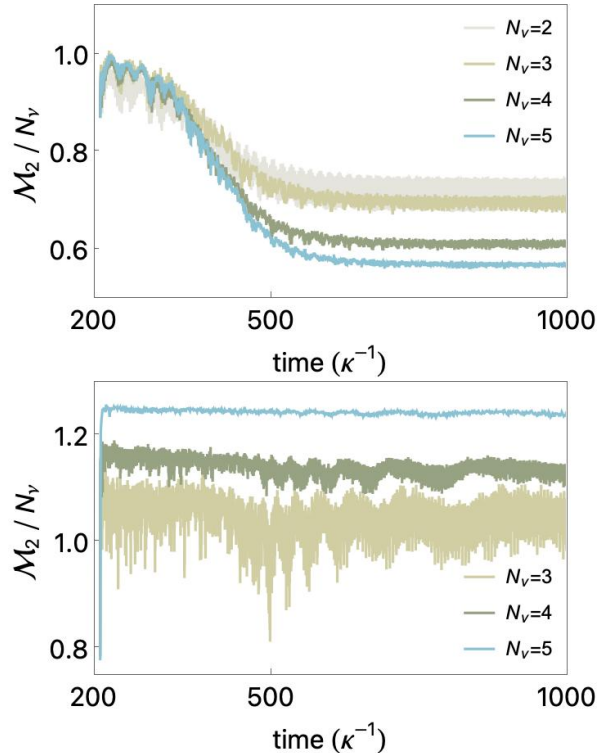


FIG. 3. \mathcal{M}_2 per neutrino in systems initially in a tensor-product states of $|\nu_e\rangle^{\otimes N_\nu}$ only (upper curves) and tensor-products of all three $|\nu_e\rangle$, $|\nu_\mu\rangle$, $|\nu_\tau\rangle$ (lower curves), as a function of time. In the case of the latter, initial states with the maximum asymptotic values of \mathcal{M}_2 from the possible flavor combinations for a given N_ν are shown, i.e., $|\nu_e\nu_\mu\nu_\tau\rangle$, $|\nu_e\nu_\mu\nu_\tau\nu_\tau\rangle$ and $|\nu_\tau\nu_\mu\nu_e\nu_\tau\nu_\mu\rangle$.

dencies of \mathcal{M}_2 for systems with $N_\nu \leq 5$ are shown in Fig. 3. Interestingly, the wavefunctions of the $|\nu_e\rangle^{\otimes N_\nu}$ initial states contain less magic than the maximum possible for a tensor-product state, $\mathcal{M}_2 \leq N_\nu$, at all times. Further, the asymptotic values are decreasing with increasing N_ν . In contrast, wavefunctions from initial states containing all three flavors support magic that exceeds the maximum value in tensor-product states, and hence necessarily requires entanglement between the neutrinos. In addition, the \mathcal{M}_2 per neutrino is increasing with increasing numbers of neutrinos, as displayed in Fig. 4 for $N_\nu \leq 8$. See App. E for the asymptotic values of \mathcal{M}_2 from a selection of initial states. The evolution of the probabilities of being in the mass eigenstates, the concurrence and generalized-concurrence, and the 2- and 4-tangles in the wavefunctions, are displayed for $|\nu_e\rangle^{\otimes 5}$ and

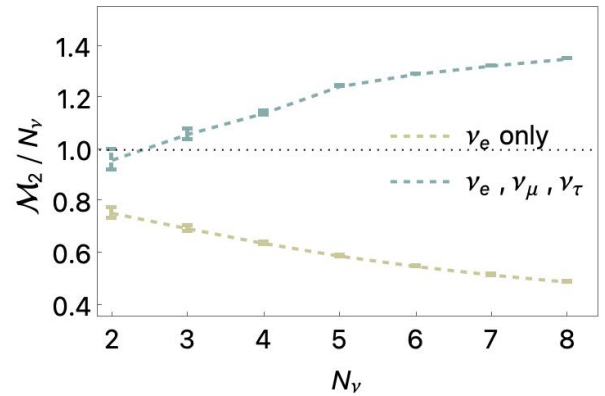


FIG. 4. The asymptotic values of \mathcal{M}_2 per neutrino in systems initially in a tensor-product state of $|\nu_e\rangle^{\otimes N_\nu}$ (brown points and dashed curve) and in systems initially in tensor-products of all three $|\nu_e\rangle$, $|\nu_\mu\rangle$, $|\nu_\tau\rangle$ (blue points and dashed curve). The maximum value of \mathcal{M}_2 from the possible flavor combinations of the initial state for a given N_ν has been chosen. The horizontal-dotted-black line corresponds to the maximum value attainable with tensor-product states. The numerical values of the displayed results are given in Table I of App. E.

$|\nu_e\nu_e\nu_\mu\nu_\mu\nu_\tau\rangle$, as examples in the $N_\nu = 5$ systems, in App. F.

With the recent advances in better understanding the roles of magic and entanglement in the computational complexity of many-body systems, this work represents a step toward quantifying the magic in dense systems of neutrinos. The combination of large-scale entanglement and large measures of magic are both necessary to conclude that quantum resources are required to prepare a state. The results that we have obtained (with the small numbers of neutrinos considered) here build upon previous results to further suggest that quantum resources will be required to prepare and evolve systems of dense neutrinos due to the scaling of the magic in the mixed-flavor channels. Quantifying the behavior of magic and multi-partite entanglement in larger systems of neutrinos is an important next step. However, this is only part of the challenge that lies ahead in describing these systems. Combining these quantum aspects of the system into realistic simulations, including scattering processes and full kinetics, remains to be accomplished. Thus, the full impact of observations made here remain to be determined.

In a broader context, there are indications that the parameters defining the Standard Model are such that the interactions are near extremal points in their entanglement power [100, 101], related to emergent symmetries [101–105], and connected to flavor structures [106]. The present work, along with what is already known about magic in strongly-interacting systems [78, 79], is highlighting their connection to the computing resources required for simulating systems of fundamental particles.

ACKNOWLEDGMENTS

We would like to thank Vincenzo Cirigliano, Henry Froland and Niklas Müller for useful discussions, as well as Emanuele Tirrito for his inspiring presentation at the IQuS workshop *Pulses, Qudits and Quantum Simulations*², co-organized by Yujin Cho, Ravi Naik, Alessandro Roggero and Kyle Wendt, and for subsequent discussions, as also related discussions with Alessandro Roggero and Kyle Wendt. We would further thank Alioscia Hamma, Thomas Papenbrock and Rahul Trivedi for useful discussions during the IQuS workshop *Entanglement in Many-Body Systems: From Nuclei to Quantum Computers and Back*³, co-organized by Mari Carmen Bañuls, Susan Coppersmith, Calvin Johnson and

Caroline Robin. This work was supported by U.S. Department of Energy, Office of Science, Office of Nuclear Physics, InQubator for Quantum Simulation (IQuS)⁴ under Award Number DOE (NP) Award DE-SC0020970 via the program on Quantum Horizons: QIS Research and Innovation for Nuclear Science⁵, and by the Department of Physics⁶ and the College of Arts and Sciences⁷ at the University of Washington (Ivan and Martin). This work was also supported, in part, by Universität Bielefeld, and by ERC-885281-KILONOVA Advanced Grant (Caroline). This research used resources of the National Energy Research Scientific Computing Center, a DOE Office of Science User Facility supported by the Office of Science of the U.S. Department of Energy under Contract No. DE-AC02-05CH11231 using NERSC awards NP-ERCAP0027114 and NP-ERCAP0029601.

-
- [1] A. Burrows and D. Vartanyan, Core-collapse supernova explosion theory, *Nature* **589**, 29–39 (2021).
 - [2] B. Müller, Neutrino emission as diagnostics of core-collapse supernovae, *Annual Review of Nuclear and Particle Science* **69**, 253 (2019).
 - [3] S. Wanajo, Y. Sekiguchi, N. Nishimura, K. Kiuchi, K. Kyutoku, and M. Shibata, Production of all the r-process nuclides in the dynamical ejecta of neutron star mergers, *The Astrophysical Journal Letters* **789**, L39 (2014).
 - [4] R. Hoffman, S. Woosley, and Y.-Z. Qian, Nucleosynthesis in neutrino-driven winds. ii. implications for heavy element synthesis, *The Astrophysical Journal* **482**, 951 (1997).
 - [5] C. Winteler, R. Kaeppli, A. Perego, A. Arcones, N. Vasset, N. Nishimura, M. Liebendoerfer, and F.-K. Thielemann, Magnetorotationally driven supernovae as the origin of early galaxy r-process elements?, *The astrophysical journal letters* **750**, L22 (2012).
 - [6] S. W. Bruenn, A. Mezzacappa, W. R. Hix, J. M. Blondin, P. Marronetti, O. E. B. Messer, C. J. Dirk, and S. Yoshida, 2D and 3D Core-Collapse Supernovae Simulation Results Obtained with the CHIMERA Code, *J. Phys. Conf. Ser.* **180**, 012018 (2009), [arXiv:1002.4914 \[astro-ph.SR\]](https://arxiv.org/abs/1002.4914).
 - [7] S. W. Bruenn, C. J. Dirk, A. Mezzacappa, J. C. Hayes, J. M. Blondin, W. R. Hix, and O. E. B. Messer, Modeling core collapse supernovae in 2 and 3 dimensions with spectral neutrino transport, *J. Phys. Conf. Ser.* **46**, 393 (2006), [arXiv:0709.0537 \[astro-ph\]](https://arxiv.org/abs/0709.0537).
 - [8] F. Foucart, Neutrino transport in general relativistic neutron star merger simulations, *Living Reviews in Computational Astrophysics* **9**, 10.1007/s41115-023-00016-y (2023).
 - [9] M. Cusinato, F. M. Guercilena, A. Perego, D. Logoteta, D. Radice, S. Bernuzzi, and S. Ansoldi, Neutrino emission from binary neutron star mergers: characterising light curves and mean energies, *The European Physical Journal A* **58**, 10.1140/epja/s10050-022-00743-5 (2022).
 - [10] V. Vijayan, A. Bauswein, and G. Martinez-Pinedo, Neutrinos and their impact on the nucleosynthesis in binary neutron star mergers, *PoS FAIRness2022*, 061 (2023).
 - [11] M. George, M.-R. Wu, I. Tamborra, R. Ardevol-Pulpillo, and H.-T. Janka, Fast neutrino flavor conversion, ejecta properties, and nucleosynthesis in newly-formed hypermassive remnants of neutron-star mergers, *Phys. Rev. D* **102**, 103015 (2020), [arXiv:2009.04046 \[astro-ph.HE\]](https://arxiv.org/abs/2009.04046).
 - [12] I. Padilla-Gay, S. Shalgar, and I. Tamborra, Symmetry breaking due to multi-angle matter-neutrino resonance in neutron star merger remnants, *JCAP* **05**, 037, [arXiv:2403.15532 \[astro-ph.HE\]](https://arxiv.org/abs/2403.15532).
 - [13] L. Johns, H. Nagakura, G. M. Fuller, and A. Burrows, Neutrino oscillations in supernovae: Angular moments and fast instabilities, *Phys. Rev. D* **101**, 043009 (2020).
 - [14] P. L. Espino, P. Hammond, D. Radice, S. Bernuzzi, R. Gamba, F. Zappa, L. F. L. Micchi, and A. Perego, Neutrino trapping and out-of-equilibrium effects in binary neutron-star merger remnants, *Phys. Rev. Lett.* **132**, 211001 (2024).
 - [15] P. L. Espino, D. Radice, F. Zappa, R. Gamba, and S. Bernuzzi, Impact of moment-based, energy integrated neutrino transport on microphysics and ejecta in binary neutron star mergers, *Phys. Rev. D* **109**, 103027 (2024).
 - [16] A. B. Balantekin, M. J. Cervia, A. V. Patwardhan, R. Surman, and X. Wang, Collective Neutrino Oscillations and Heavy-element Nucleosynthesis in Supernovae: Exploring Potential Effects of Many-body Neutrino Correlations, *Astrophys. J.* **967**, 146 (2024), [arXiv:2311.02562 \[astro-ph.HE\]](https://arxiv.org/abs/2311.02562).
 - [17] M. Cornelius, S. Shalgar, and I. Tamborra, Neutrino quantum kinetics in two spatial dimensions, (2024), [arXiv:2407.04769 \[astro-ph.HE\]](https://arxiv.org/abs/2407.04769).
 - [18] S. Shalgar and I. Tamborra, Neutrino quantum ki-

² <https://iqus.uw.edu/events/pulsesquditssimulations/>

³ <https://iqus.uw.edu/events/entanglementinmanybody/>

⁴ <https://iqus.uw.edu>

⁵ <https://science.osti.gov/np/Research/Quantum-Information-Science>

⁶ <https://phys.washington.edu>

⁷ <https://www.artsci.washington.edu>

- netics in a core-collapse supernova, *JCAP* **09**, 021, [arXiv:2406.09504 \[astro-ph.HE\]](#).
- [19] A. M. Suliga, P. C.-K. Cheong, J. Froustey, G. M. Fuller, L. Gráf, K. Kehrer, O. Scholer, and S. Shalgar, Non-conservation of Lepton Numbers in the Neutrino Sector Could Change the Prospects for Core Collapse Supernova Explosions, (2024), [arXiv:2410.01080 \[hep-ph\]](#).
- [20] Y. Z. Qian and G. M. Fuller, Neutrino-neutrino scattering and matter enhanced neutrino flavor transformation in Supernovae, *Phys. Rev. D* **51**, 1479 (1995), [arXiv:astro-ph/9406073](#).
- [21] H. Duan, G. M. Fuller, J. Carlson, and Y.-Z. Qian, Coherent Development of Neutrino Flavor in the Supernova Environment, *Phys. Rev. Lett.* **97**, 241101 (2006), [arXiv:astro-ph/0608050](#).
- [22] H. Duan, G. M. Fuller, J. Carlson, and Y.-Z. Qian, Simulation of Coherent Non-Linear Neutrino Flavor Transformation in the Supernova Environment. 1. Correlated Neutrino Trajectories, *Phys. Rev. D* **74**, 105014 (2006), [arXiv:astro-ph/0606616](#).
- [23] I. Izaguirre, G. Raffelt, and I. Tamborra, Fast Pairwise Conversion of Supernova Neutrinos: A Dispersion-Relation Approach, *Phys. Rev. Lett.* **118**, 021101 (2017), [arXiv:1610.01612 \[hep-ph\]](#).
- [24] F. Capozzi, M. Chakraborty, S. Chakraborty, and M. Sen, Fast flavor conversions in supernovae: the rise of mu-tau neutrinos, *Phys. Rev. Lett.* **125**, 251801 (2020), [arXiv:2005.14204 \[hep-ph\]](#).
- [25] D. F. G. Fiorillo and G. G. Raffelt, Slow and fast collective neutrino oscillations: Invariants and reciprocity, *Phys. Rev. D* **107**, 043024 (2023), [arXiv:2301.09650 \[hep-ph\]](#).
- [26] D. F. G. Fiorillo and G. G. Raffelt, Flavor solitons in dense neutrino gases, *Phys. Rev. D* **107**, 123024 (2023), [arXiv:2303.12143 \[hep-ph\]](#).
- [27] D. F. G. Fiorillo, G. G. Raffelt, and G. Sigl, Inhomogeneous Kinetic Equation for Mixed Neutrinos: Tracing the Missing Energy, *Phys. Rev. Lett.* **133**, 021002 (2024), [arXiv:2401.05278 \[hep-ph\]](#).
- [28] S. Shalgar and I. Tamborra, Do we have enough evidence to invalidate the mean-field approximation adopted to model collective neutrino oscillations?, *Phys. Rev. D* **107**, 123004 (2023), [arXiv:2304.13050 \[astro-ph.HE\]](#).
- [29] L. Johns, Neutrino many-body correlations (2023), [arXiv:2305.04916 \[hep-ph\]](#).
- [30] E. Rrapaj, Exact solution of multiangle quantum many-body collective neutrino-flavor oscillations, *Phys. Rev. C* **101**, 065805 (2020), [arXiv:1905.13335 \[hep-ph\]](#).
- [31] A. V. Patwardhan, M. J. Cervia, and A. B. Balantekin, Eigenvalues and eigenstates of the many-body collective neutrino oscillation problem, *Phys. Rev. D* **99**, 123013 (2019).
- [32] A. V. Patwardhan, M. J. Cervia, and A. B. Balantekin, Spectral splits and entanglement entropy in collective neutrino oscillations, *Phys. Rev. D* **104**, 123035 (2021), [arXiv:2109.08995 \[hep-ph\]](#).
- [33] A. Roggero, Entanglement and many-body effects in collective neutrino oscillations, *Phys. Rev. D* **104**, 103016 (2021), [arXiv:2102.10188 \[hep-ph\]](#).
- [34] Z. Xiong, Many-body effects of collective neutrino oscillations, *Phys. Rev. D* **105**, 103002 (2022), [arXiv:2111.00437 \[astro-ph.HE\]](#).
- [35] A. Roggero, Dynamical phase transitions in models of collective neutrino oscillations, *Phys. Rev. D* **104**, 123023 (2021), [arXiv:2103.11497 \[hep-ph\]](#).
- [36] J. D. Martin, A. Roggero, H. Duan, J. Carlson, and V. Cirigliano, Classical and quantum evolution in a simple coherent neutrino problem, *Phys. Rev. D* **105**, 083020 (2022), [arXiv:2112.12686 \[hep-ph\]](#).
- [37] A. Roggero, E. Rrapaj, and Z. Xiong, Entanglement and correlations in fast collective neutrino flavor oscillations, *Phys. Rev. D* **106**, 043022 (2022), [arXiv:2203.02783 \[astro-ph.HE\]](#).
- [38] M. Illa and M. J. Savage, Multi-Neutrino Entanglement and Correlations in Dense Neutrino Systems, *Phys. Rev. Lett.* **130**, 221003 (2023), [arXiv:2210.08656 \[nucl-th\]](#).
- [39] R. Bhaskar, A. Roggero, and M. J. Savage, Time Scales in Many-Body Fast Neutrino Flavor Conversion (2023), [arXiv:2312.16212 \[nucl-th\]](#).
- [40] J. D. Martin, D. Neill, A. Roggero, H. Duan, and J. Carlson, Equilibration of quantum many-body fast neutrino flavor oscillations, *Phys. Rev. D* **108**, 123010 (2023), [arXiv:2307.16793 \[hep-ph\]](#).
- [41] J. D. Martin, A. Roggero, H. Duan, and J. Carlson, Many-body neutrino flavor entanglement in a simple dynamic model, (2023), [arXiv:2301.07049 \[hep-ph\]](#).
- [42] D. Neill, H. Liu, J. Martin, and A. Roggero, Scattering Neutrinos, Spin Models, and Permutations (2024), [arXiv:2406.18677 \[hep-ph\]](#).
- [43] A. Kost, L. Johns, and H. Duan, Once-in-a-lifetime encounter models for neutrino media: From coherent oscillations to flavor equilibration, *Phys. Rev. D* **109**, 103037 (2024), [arXiv:2402.05022 \[hep-ph\]](#).
- [44] V. Cirigliano, S. Sen, and Y. Yamauchi, Neutrino many-body flavor evolution: the full Hamiltonian (2024), [arXiv:2404.16690 \[hep-ph\]](#).
- [45] A. B. Balantekin and Y. Pehlivan, Neutrino-Neutrino Interactions and Flavor Mixing in Dense Matter, *J. Phys. G* **34**, 47 (2007), [arXiv:astro-ph/0607527](#).
- [46] P. Siwach, A. M. Suliga, and A. B. Balantekin, Entanglement in three-flavor collective neutrino oscillations, *Phys. Rev. D* **107**, 023019 (2023), [arXiv:2211.07678 \[hep-ph\]](#).
- [47] A. B. Balantekin, M. J. Cervia, A. V. Patwardhan, E. Rrapaj, and P. Siwach, Quantum information and quantum simulation of neutrino physics, *Eur. Phys. J. A* **59**, 186 (2023), [arXiv:2305.01150 \[nucl-th\]](#).
- [48] I. A. Chernyshev, Three-flavor Collective Neutrino Oscillations on D-Wave's Advantage Quantum Annealer (2024), [arXiv:2405.20436 \[quant-ph\]](#).
- [49] F. Turro, I. A. Chernyshev, R. Bhaskar, and M. Illa, Qutrit and Qubit Circuits for Three-Flavor Collective Neutrino Oscillations, (2024), [arXiv:2407.13914 \[quant-ph\]](#).
- [50] B. Hall, A. Roggero, A. Baroni, and J. Carlson, Simulation of collective neutrino oscillations on a quantum computer, *Phys. Rev. D* **104**, 063009 (2021), [arXiv:2102.12556 \[quant-ph\]](#).
- [51] K. Yeter-Aydeniz, S. Bangar, G. Siopsis, and R. C. Pooser, Collective neutrino oscillations on a quantum computer, *Quantum Inf. Process* **21**, 84 (2022), [arXiv:2104.03273 \[quant-ph\]](#).
- [52] M. Illa and M. J. Savage, Basic elements for simulations of standard-model physics with quantum annealers: Multigrid and clock states, *Phys. Rev. A* **106**, 052605 (2022), [arXiv:2202.12340 \[quant-ph\]](#).
- [53] V. Amitrano, A. Roggero, P. Luchi, F. Turro,

- L. Vespucci, and F. Pederiva, Trapped-ion quantum simulation of collective neutrino oscillations, *Phys. Rev. D* **107**, 023007 (2023), [arXiv:2207.03189 \[quant-ph\]](#).
- [54] P. Siwach, K. Harrison, and A. B. Balantekin, Collective neutrino oscillations on a quantum computer with hybrid quantum-classical algorithm, *Phys. Rev. D* **108**, 083039 (2023), [arXiv:2308.09123 \[quant-ph\]](#).
- [55] D. Gottesman, The Heisenberg representation of quantum computers (1998), [arXiv:quant-ph/9807006 \[quant-ph\]](#).
- [56] S. Aaronson and D. Gottesman, Improved simulation of stabilizer circuits, *Physical Review A* **70**, 10.1103/physreva.70.052328 (2004).
- [57] D. Gottesman, Stabilizer codes and quantum error correction (1997), [arXiv:quant-ph/9705052 \[quant-ph\]](#).
- [58] V. Kashyap, G. Styliaris, S. Mouradian, J. I. Cirac, and R. Trivedi, Accuracy guarantees and quantum advantage in analogue open quantum simulation with and without noise, (2024), [arXiv:2404.11081 \[quant-ph\]](#).
- [59] J. Emerson, D. Gottesman, S. A. H. Mousavian, and V. Veitch, The resource theory of stabilizer quantum computation, *New J. Phys.* **16**, 013009 (2014), [arXiv:1307.7171 \[quant-ph\]](#).
- [60] X. Wang, M. M. Wilde, and Y. Su, Efficiently computable bounds for magic state distillation, *Phys. Rev. Lett.* **124**, 090505 (2020).
- [61] M. Howard and E. Campbell, Application of a resource theory for magic states to fault-tolerant quantum computing, *Phys. Rev. Lett.* **118**, 090501 (2017).
- [62] S. Bravyi, D. Browne, P. Calpin, E. Campbell, D. Gosset, and M. Howard, Simulation of quantum circuits by low-rank stabilizer decompositions, *Quantum* **3**, 181 (2019).
- [63] E. T. Campbell, Catalysis and activation of magic states in fault-tolerant architectures, *Phys. Rev. A* **83**, 032317 (2011).
- [64] M. Beverland, E. Campbell, M. Howard, and V. Kliuchnikov, Lower bounds on the non-Clifford resources for quantum computations, *Quantum Sci. Technol.* **5**, 035009 (2020), [arXiv:1904.01124 \[quant-ph\]](#).
- [65] L. Leone, S. F. E. Oliviero, and A. Hamma, Stabilizer Renyi Entropy, *Phys. Rev. Lett.* **128**, 050402 (2022), [arXiv:2106.12587 \[quant-ph\]](#).
- [66] T. Haug and M. Kim, Scalable measures of magic resource for quantum computers, *PRX Quantum* **4**, 010301 (2023).
- [67] S. F. E. Oliviero, L. Leone, A. Hamma, and S. Lloyd, Measuring magic on a quantum processor, *npj Quantum Information* **8**, 10.1038/s41534-022-00666-5 (2022).
- [68] D. Bluvstein *et al.*, Logical quantum processor based on reconfigurable atom arrays, *Nature* **626**, 58 (2024), [arXiv:2312.03982 \[quant-ph\]](#).
- [69] T. Haug and L. Piroli, Quantifying nonstabilizerness of matrix product states, *Phys. Rev. B* **107**, 035148 (2023), [arXiv:2207.13076 \[quant-ph\]](#).
- [70] T. Haug and L. Piroli, Stabilizer entropies and non-stabilizerness monotones, *Quantum* **7**, 1092 (2023), [arXiv:2303.10152 \[quant-ph\]](#).
- [71] P. S. Tarabunga, E. Tirrito, M. C. Bañuls, and M. Dalmonte, Nonstabilizerness via Matrix Product States in the Pauli Basis, *Phys. Rev. Lett.* **133**, 010601 (2024), [arXiv:2401.16498 \[quant-ph\]](#).
- [72] G. Lami, T. Haug, and J. D. Nardis, Quantum state designs with clifford enhanced matrix product states (2024), [arXiv:2404.18751 \[quant-ph\]](#).
- [73] D. Rattacaso, L. Leone, S. F. E. Oliviero, and A. Hamma, Stabilizer entropy dynamics after a quantum quench, *Phys. Rev. A* **108**, 042407 (2023), [arXiv:2304.13768 \[quant-ph\]](#).
- [74] M. Frau, P. S. Tarabunga, M. Collura, M. Dalmonte, and E. Tirrito, Non-stabilizerness versus entanglement in matrix product states (2024), [arXiv:2404.18768 \[quant-ph\]](#).
- [75] A. G. Catalano, J. Odavić, G. Torre, A. Hamma, F. Franchini, and S. M. Giampaolo, Magic phase transition and non-local complexity in generalized W State, (2024), [arXiv:2406.19457 \[quant-ph\]](#).
- [76] P. S. Tarabunga, E. Tirrito, T. Chanda, and M. Dalmonte, Many-Body Magic Via Pauli-Markov Chains—From Criticality to Gauge Theories, *PRX Quantum* **4**, 040317 (2023), [arXiv:2305.18541 \[quant-ph\]](#).
- [77] S. Cepollaro, G. Chirco, G. Cuffaro, G. Esposito, and A. Hamma, Stabilizer entropy of quantum tetrahedra, (2024), [arXiv:2402.07843 \[hep-th\]](#).
- [78] C. E. P. Robin and M. J. Savage, The Magic in Nuclear and Hypernuclear Forces, (2024), [arXiv:2405.10268 \[nucl-th\]](#).
- [79] F. Brokemeier, S. M. Hengstenberg, J. W. T. Keeble, C. E. P. Robin, F. Rocco, and M. J. Savage, Quantum Magic and Multi-Partite Entanglement in the Structure of Nuclei, (2024), [arXiv:2409.12064 \[nucl-th\]](#).
- [80] G. E. Fux, E. Tirrito, M. Dalmonte, and R. Fazio, Entanglement-magic separation in hybrid quantum circuits, (2023), [arXiv:2312.02039 \[quant-ph\]](#).
- [81] M. Bejan, C. McLauchlan, and B. Béri, Dynamical Magic Transitions in Monitored Clifford+T Circuits, (2023), [arXiv:2312.00132 \[quant-ph\]](#).
- [82] G. Li *et al.*, Measurement Induced Magic Resources, (2024), [arXiv:2408.01980 \[quant-ph\]](#).
- [83] M. Howard, E. Brennan, and J. Vala, Quantum contextuality with stabilizer states, *Entropy* **15**, 2340–2362 (2013).
- [84] S. X. Cui and Z. Wang, Universal quantum computation with metaplectic anyons, *Journal of Mathematical Physics* **56**, 10.1063/1.4914941 (2015).
- [85] Q. Wang, Qutrit zx-calculus is complete for stabilizer quantum mechanics, *Electronic Proceedings in Theoretical Computer Science* **266**, 58 (2018).
- [86] H. Zhu, R. Kueng, M. Grassl, and D. Gross, The clifford group fails gracefully to be a unitary 4-design (2016), [arXiv:1609.08172 \[quant-ph\]](#).
- [87] L. Leone and L. Bittel, Stabilizer entropies are monotones for magic-state resource theory, (2024), [arXiv:2404.11652 \[quant-ph\]](#).
- [88] B. Pontecorvo, Mesonium and antimesonium, *Sov. Phys. JETP* **6**, 429 (1957), originally published in *J. Exptl. Theoret. Phys. (U.S.S.R.)* **33**, 549–551 (1957).
- [89] Z. Maki, M. Nakagawa, and S. Sakata, Remarks on the unified model of elementary particles, *Prog. Theor. Phys.* **28**, 870 (1962).
- [90] S. Navas *et al.* (Particle Data Group), Review of particle physics, *Phys. Rev. D* **110**, 030001 (2024).
- [91] G. M. Fuller, R. W. Mayle, J. R. Wilson, and D. N. Schramm, Resonant neutrino oscillations and stellar collapse, *Astrophys. J.* **322**, 795 (1987).
- [92] M. J. Savage, R. A. Malaney, and G. M. Fuller, Neutrino Oscillations and the Leptonic Charge of the Universe,

- Astrophys. J.* **368**, 1 (1991).
- [93] J. T. Pantaleone, Neutrino oscillations at high densities, *Phys. Lett. B* **287**, 128 (1992).
- [94] J. Pantaleone, Dirac neutrinos in dense matter, *Phys. Rev. D* **46**, 510 (1992).
- [95] R. A. Malaney and G. J. Mathews, Probing the early universe: A Review of primordial nucleosynthesis beyond the standard Big Bang, *Phys. Rept.* **229**, 145 (1993).
- [96] V. A. Kostelecky, J. T. Pantaleone, and S. Samuel, Neutrino oscillation in the early universe, *Phys. Lett. B* **315**, 46 (1993).
- [97] J. C. D’Olivo and J. F. Nieves, Field theoretic treatment of mixed neutrinos in a neutrino and matter background, (1995), [arXiv:hep-ph/9501327](https://arxiv.org/abs/hep-ph/9501327).
- [98] Y.-Z. Qian and G. M. Fuller, Signature of supernova neutrino flavor mixing in water Cherenkov detectors, *Phys. Rev. D* **49**, 1762 (1994).
- [99] G. M. Fuller and Y.-Z. Qian, Simultaneous flavor transformation of neutrinos and antineutrinos with dominant potentials from neutrino-neutrino forward scattering, *Phys. Rev. D* **73**, 023004 (2006), [arXiv:astro-ph/0505240](https://arxiv.org/abs/astro-ph/0505240).
- [100] A. Cervera-Lierta, J. I. Latorre, J. Rojo, and L. Rottoli, Maximal Entanglement in High Energy Physics, *SciPost Phys.* **3**, 036 (2017), [arXiv:1703.02989](https://arxiv.org/abs/1703.02989) [hep-th].
- [101] S. R. Beane, D. B. Kaplan, N. Klco, and M. J. Savage, Entanglement Suppression and Emergent Symmetries of Strong Interactions, *Phys. Rev. Lett.* **122**, 102001 (2019), [arXiv:1812.03138](https://arxiv.org/abs/1812.03138) [nucl-th].
- [102] S. R. Beane, R. C. Farrell, and M. Varma, Entanglement minimization in hadronic scattering with pions, *Int. J. Mod. Phys. A* **36**, 2150205 (2021), [arXiv:2108.00646](https://arxiv.org/abs/2108.00646) [hep-ph].
- [103] Q. Liu, I. Low, and T. Mehen, Minimal entanglement and emergent symmetries in low-energy qcd, *Phys. Rev. C* **107**, 025204 (2023).
- [104] Q. Liu and I. Low, Hints of entanglement suppression in hyperon-nucleon scattering (2023), [arXiv:2312.02289](https://arxiv.org/abs/2312.02289) [hep-ph].
- [105] G. A. Miller, Entanglement maximization in low-energy neutron-proton scattering, *Phys. Rev. C* **108**, L031002 (2023), [arXiv:2306.03239](https://arxiv.org/abs/2306.03239) [nucl-th].
- [106] J. Thaler and S. Trifinopoulos, Flavor Patterns of Fundamental Particles from Quantum Entanglement?, (2024), [arXiv:2410.23343](https://arxiv.org/abs/2410.23343) [hep-ph].
- [107] D. Gross, Hudson’s theorem for finite-dimensional quantum systems, *Journal of Mathematical Physics* **47**, 10.1063/1.2393152 (2006).
- [108] H. J. García, I. L. Markov, and A. W. Cross, On the geometry of stabilizer states, *Quantum Info. Comput.* **14**, 683–720 (2014), [arXiv:1711.07848](https://arxiv.org/abs/1711.07848) [quant-ph].
- [109] Z.-H. Chen, Z.-H. Ma, O. Günhe, and S. Severini, Estimating entanglement monotones with a generalization of the wootters formula, *Physical Review Letters* **109**, 10.1103/physrevlett.109.200503 (2012).

Appendix A: Stabilizer States

Stabilizer states can be generated by repeated applications of the classical gate set on a tensor-product state, or another stabilizer state. The classical gate set can be defined in terms of the Hadamard gate, H , the phase gate, S , and CNOT gates. The number of stabilizer states can be computed exactly for a given number of qudits [56, 107, 108]: $\mathbf{d}(\mathbf{d} + 1)$ for 1 qudit, $\mathbf{d}^2(\mathbf{d} + 1)(\mathbf{d}^2 + 1)$ for 2 qudits, $\mathbf{d}^3(\mathbf{d} + 1)(\mathbf{d}^2 + 1)(\mathbf{d}^3 + 1)$ for 3 qudits, and so forth. Thus there are 6, 60, 1080, \dots stabilizer states for qubits ($\mathbf{d} = 2$), and 12, 360, 30240, \dots stabilizer states for qutrits ($\mathbf{d} = 3$).

The single-qubit H-gate and S-gate, and the two-qubit CNOT $_{ij}$ -gates (a two-qubit control-X entangling gate where i denotes the control qubit and j the target qubit), are given by, for example,

$$H = \frac{1}{\sqrt{2}} \begin{pmatrix} 1 & 1 \\ 1 & -1 \end{pmatrix}, \quad S = \begin{pmatrix} 1 & 0 \\ 0 & i \end{pmatrix}, \quad \text{CNOT}_{12} = \begin{pmatrix} 1 & 0 & 0 & 0 \\ 0 & 1 & 0 & 0 \\ 0 & 0 & 0 & 1 \\ 0 & 0 & 1 & 0 \end{pmatrix}. \quad (\text{A1})$$

Generalizing to qutrits, the single-qutrit H-gate and S-gate, and the two-qutrit CNOT $_{ij}$ -gates can be given by,

$$\hat{H} = \frac{1}{\sqrt{3}} \begin{pmatrix} 1 & 1 & 1 \\ 1 & \omega & \omega^2 \\ 1 & \omega^2 & \omega \end{pmatrix}, \quad \hat{S} = \begin{pmatrix} 1 & 0 & 0 \\ 0 & 1 & 0 \\ 0 & 0 & \omega \end{pmatrix}, \quad \omega = e^{i2\pi/3}, \quad (\text{A2})$$

and

$$\text{CNOT}_{12}|a, b\rangle = |a, a + b \bmod(3)\rangle. \quad (\text{A3})$$

The latter is implemented using projectors and shift operators, as in the case of qubits. For example, CNOT $_{12}$ has matrix representation

$$\begin{aligned} \text{CNOT}_{12} &= \hat{\Lambda}_0 \otimes \hat{I}_3 + \hat{\Lambda}_1 \otimes \hat{R}_1 + \hat{\Lambda}_2 \otimes \hat{R}_2, \\ \hat{\Lambda}_0 &= \begin{pmatrix} 1 & 0 & 0 \\ 0 & 0 & 0 \\ 0 & 0 & 0 \end{pmatrix}, \quad \hat{\Lambda}_1 = \begin{pmatrix} 0 & 0 & 0 \\ 0 & 1 & 0 \\ 0 & 0 & 0 \end{pmatrix}, \quad \hat{\Lambda}_2 = \begin{pmatrix} 0 & 0 & 0 \\ 0 & 0 & 0 \\ 0 & 0 & 1 \end{pmatrix}, \\ \hat{R}_1 &= \begin{pmatrix} 0 & 0 & 1 \\ 1 & 0 & 0 \\ 0 & 1 & 0 \end{pmatrix}, \quad \hat{R}_2 = \begin{pmatrix} 0 & 1 & 0 \\ 0 & 0 & 1 \\ 1 & 0 & 0 \end{pmatrix}. \end{aligned} \quad (\text{A4})$$

A universal quantum gate set can be formed by including T -gates, which for qubits and qutrits are, respectively,

$$\hat{T}_2 = \begin{pmatrix} 1 & 0 \\ 0 & e^{i\pi/4} \end{pmatrix}, \quad \hat{T}_3 = \begin{pmatrix} 1 & 0 & 0 \\ 0 & e^{\frac{2i\pi}{9}} & 0 \\ 0 & 0 & e^{-\frac{2i\pi}{9}} \end{pmatrix}. \quad (\text{A5})$$

The single-qubit stabilizer states are,

$$\left\{ (1, 0), (0, 1), \frac{1}{\sqrt{2}}(1, 1), \frac{1}{\sqrt{2}}(1, -1), \frac{1}{\sqrt{2}}(1, i), \frac{1}{\sqrt{2}}(1, -i) \right\}, \quad (\text{A6})$$

and the single-qutrit stabilizer states are,

$$\begin{aligned} &\{ (1, 0, 0), (0, 1, 0), (0, 0, 1), \\ &\frac{1}{\sqrt{3}}(1, 1, 1), \frac{1}{\sqrt{3}}(1, 1, \omega), \frac{1}{\sqrt{3}}(1, 1, \omega^2), \frac{1}{\sqrt{3}}(1, \omega, 1), \frac{1}{\sqrt{3}}(1, \omega^2, 1) \\ &\frac{1}{\sqrt{3}}(1, \omega, \omega), \frac{1}{\sqrt{3}}(1, \omega, \omega^2), \frac{1}{\sqrt{3}}(1, \omega^2, \omega), \frac{1}{\sqrt{3}}(1, \omega^2, \omega^2) \}. \end{aligned} \quad (\text{A7})$$

Appendix B: Computing Magic in a Quantum State

The magic in a wavefunction encoded in qudits can be straightforwardly computed in principle, but with the classical computational resources increasing exponentially with system size. Here, we present the established ‘‘in-principle’’ method for qubits and qutrits, and which can be extended to arbitrary \mathbf{d} .

1. Qubits

To quantify the magic in a qubit-supported wavefunction, we compute the stabilizer Rényi entropies (SREs) [65]. An arbitrary density matrix can be written in terms of Pauli strings,

$$\hat{\rho} = \frac{1}{d} \sum_{\hat{P} \in \tilde{\mathcal{G}}_{n_Q}} c_P \hat{P}, \quad (\text{B1})$$

where $d = 2^{n_Q}$ and $c_P = \text{Tr} \hat{\rho} \hat{P}$. $\tilde{\mathcal{G}}_{n_Q}$ is the subgroup of the generalized Pauli group \mathcal{G}_{n_Q} ,

$$\mathcal{G}_{n_Q} = \{\varphi \hat{\sigma}^{(1)} \otimes \hat{\sigma}^{(2)} \otimes \dots \otimes \hat{\sigma}^{(n_Q)}\}, \quad (\text{B2})$$

where $\hat{\sigma}^{(j)} \in \{\mathbb{1}^{(j)}, \hat{\sigma}_x^{(j)}, \hat{\sigma}_y^{(j)}, \hat{\sigma}_z^{(j)}\}$ act on qubit j and $\varphi \in \{\pm 1, \pm i\}$, with phases chosen to be $\varphi = +1$. It can be shown that [65] the quantity

$$\Xi_P \equiv \frac{c_P^2}{d}, \quad (\text{B3})$$

is a probability distribution for pure states, corresponding to the probability for $\hat{\rho}$ to be in \hat{P} . If $|\Psi\rangle$ is a stabilizer state, the expansion coefficients $c_P = \pm 1$ for d commuting Pauli strings $\hat{P} \in \tilde{\mathcal{G}}_{n_Q}$, and $c_P = 0$ for the remaining $d^2 - d$ strings [86]. Therefore, $\Xi_P = 1/d$ or 0 for a qubit stabilizer state, and the stabilizer α -Rényi entropies [65],

$$\mathcal{M}_\alpha(|\Psi\rangle) = -\log_2 d + \frac{1}{1-\alpha} \log_2 \left(\sum_{\hat{P} \in \tilde{\mathcal{G}}_{n_Q}} \Xi_P^\alpha \right), \quad (\text{B4})$$

which vanish for stabilizer states, are measures of magic in the state. It has been shown that $\alpha \geq 2$ SREs are magic monotones for pure states, in contrast to those with $\alpha < 2$ [70, 87]. Three commonly utilized measures of magic from the SREs are

$$\mathcal{M}_{lin} = 1 - d \sum_{\hat{P} \in \tilde{\mathcal{G}}_{n_Q}} \Xi_P^2, \quad \mathcal{M}_1 = - \sum_{\hat{P} \in \tilde{\mathcal{G}}_{n_Q}} \Xi_P \log_2 d \Xi_P, \quad \mathcal{M}_2 = -\log_2 d \sum_{\hat{P} \in \tilde{\mathcal{G}}_{n_Q}} \Xi_P^2. \quad (\text{B5})$$

2. Qutrits

The formulation of measures of magic for qutrits is similar to that for qubits. Instead of using the Gell-Mann matrices to define the generators of $\text{SU}(3)$, the generalized \hat{X} and \hat{Z} operators are more widely used because of their properties under tracing. Strings of Pauli operators can be written as

$$\hat{P}_{i_1, i_2, \dots, i_{n_Q}} = \hat{\Sigma}_{i_1} \otimes \hat{\Sigma}_{i_2} \otimes \dots \otimes \hat{\Sigma}_{i_{n_Q}}, \quad (\text{B6})$$

where the nine Pauli operators for qutrits (including the identity), written in terms of \hat{X} and \hat{Z} operators, are

$$\hat{\Sigma}_i \in \{\hat{I}, \hat{X}, \hat{Z}, \hat{X}^2, \omega \hat{X} \hat{Z}, \hat{Z}^2, \omega^2 \hat{X} \hat{Z}^2, \hat{X}^2 \hat{Z}, \hat{X}^2 \hat{Z}^2\}, \quad (\text{B7})$$

with

$$\hat{X}|j\rangle = |j+1\rangle \rightarrow \begin{pmatrix} 0 & 0 & 1 \\ 1 & 0 & 0 \\ 0 & 1 & 0 \end{pmatrix}, \quad \hat{Z}|j\rangle = \omega^j |j\rangle \rightarrow \begin{pmatrix} 1 & 0 & 0 \\ 0 & \omega & 0 \\ 0 & 0 & \omega^2 \end{pmatrix}. \quad (\text{B8})$$

The Pauli operators in Eq. (B7) are normalized such that

$$\text{Tr} \hat{\Sigma}_i \hat{\Sigma}_j = 3K_{ij}, \quad \text{with } K_{11} = K_{24} = K_{36} = K_{42} = K_{59} = K_{63} = K_{78} = K_{87} = K_{95} = 1, \quad \text{else } K_{ij} = 0, \quad (\text{B9})$$

where $1 + \omega + \omega^2 = 0$ has been used.

An arbitrary density matrix for a wavefunction supported on n_Q qutrits can be decomposed into sums of products of Pauli strings,

$$\hat{\rho} = \frac{1}{d} \sum_{i_a, j_b} \text{Tr} \left[\hat{\rho} \hat{P}_{i_1, i_2, \dots, i_{n_Q}} \right] K_{i_1, j_1} K_{i_2, j_2} \cdots K_{i_{n_Q}, j_{n_Q}} \hat{P}_{j_1, j_2, \dots, j_{n_Q}} , \quad (\text{B10})$$

where $d = 3^{n_Q}$.⁸

To determine the magic in a given pure state, the forward matrix elements of all Pauli strings are formed, $c_P \equiv \langle \Psi | \hat{P} | \Psi \rangle$. For stabilizer states, d of the strings give $c_P = 1, \omega$ or ω^2 , while the other $d^2 - d$ give $c_P = 0$. However, in general, for an arbitrary state, all d^2 values will *a priori* be nonzero. As is the case for qubits, described above, we can define the deviation from stabilizerness in a given state as the magic, using

$$\Xi_P = |c_P|^2/d , \quad \sum_P \Xi_P = 1 . \quad (\text{B12})$$

3. The Magic in Entangled Versus Tensor-Product States

It is known that entangled states can support more magic than non-entangled states⁹. As an example, in the case of a two-qubit system, straightforward calculations demonstrate that the maximum \mathcal{M}_2 that a tensor-product state can contain is $\mathcal{M}_2 = 1.16993$ (consistent with twice the value for a single two-flavor neutrino), while entangled states can contain up to $\mathcal{M}_2 = 1.19265$. For the two-qutrit system, explicit calculation gives a maximum value of magic in a tensor-product state of $\mathcal{M}_2 = 2$ (consistent with $2 \times$ the maximum value for a single three-flavor neutrino), while entangled states can support a maximum value of $\mathcal{M}_2 = 2.23379$.

Appendix C: The One Neutrino Sector

The neutrino flavor and mass eigenstates are related by the Pontecorvo–Maki–Nakagawa–Sakata (PMNS) matrix [88, 89],

$$\boldsymbol{\nu}_F = U_{PMNS} \boldsymbol{\nu}_M , \quad (\text{C1})$$

where $\boldsymbol{\nu}_F = (\nu_e, \nu_\mu, \nu_\tau)^T$ and $\boldsymbol{\nu}_M = (\nu_1, \nu_2, \nu_3)^T$ are the three-component vectors of neutrino fields in the flavor and mass bases, respectively. In a common parameterization, the PMNS mixing matrix can be written as (without Majorana phases),

$$U_{PMNS} = \begin{pmatrix} 1 & 0 & 0 \\ 0 & \cos \theta_{23} & \sin \theta_{23} \\ 0 & -\sin \theta_{23} & \cos \theta_{23} \end{pmatrix} \begin{pmatrix} \cos \theta_{13} & 0 & e^{-i\delta} \sin \theta_{13} \\ 0 & 1 & 0 \\ -e^{+i\delta} \sin \theta_{13} & 0 & \cos \theta_{13} \end{pmatrix} \begin{pmatrix} \cos \theta_{12} & \sin \theta_{12} & 0 \\ -\sin \theta_{12} & \cos \theta_{12} & 0 \\ 0 & 0 & 1 \end{pmatrix} , \quad (\text{C2})$$

where the experimentally determined angles are [90],

$$\sin^2 \theta_{12} = 0.307 \pm 0.013, \quad \sin^2 \theta_{23} = 0.553_{-0.024}^{+0.016}, \quad \sin^2 \theta_{13} = (2.19 \pm 0.07) \times 10^{-2}, \quad \delta = (1.19 \pm 0.22) \pi \text{ rad} . \quad (\text{C3})$$

The neutrino mass-squared differences are known experimentally to be [90],

$$\delta m_{21}^2 = (7.53 \pm 0.18) \times 10^{-17} \text{ MeV}^2 , \quad \Delta m_{32}^2 = (2.455 \pm 0.028) \times 10^{-15} \text{ MeV}^2 \text{ [normal]} . \quad (\text{C4})$$

We are only considering the normal hierarchy of neutrino masses and not the inverted hierarchy. While the above mixing and masses are in the case of three neutrinos, the (commonly considered) effective two-neutrino sector is found by using the θ_{12} mixing angle and δm_{21}^2 mass-squared difference.

⁸ There is a useful relation between sums of operators

$$\sum_{a=1}^8 \hat{T}^a \otimes \hat{T}^a = \frac{2}{3} \sum_{a,b=2}^9 \hat{\Sigma}_a \otimes \hat{\Sigma}_b K_{a,b} . \quad (\text{B11})$$

⁹ We thank Alioscia Hama for making this point to us.

With these experimental values, the mixing matrices for the effective two-flavor and three-flavor systems become

$$U_2 = \begin{pmatrix} 0.8324(78) & 0.554(12) \\ -0.554(12) & 0.8324(78) \end{pmatrix},$$

$$U_{PMNS} = \begin{pmatrix} 0.8233(77) & 0.548(12) & -0.096(57) + i0.065(71) \\ -0.311(37) + i0.041(44) & 0.596(27) + i0.027(29) & 0.735(13) \\ 0.466(33) + i0.036(40) & -0.583(25) + i0.024(26) & 0.661(15) \end{pmatrix}, \quad (\text{C5})$$

respectively. When evaluated at the mean values of the angles and phase, the mixing matrices are,

$$U_2 = \begin{pmatrix} 0.832466 & 0.554076 \\ -0.554076 & 0.832466 \end{pmatrix},$$

$$U_{PMNS} = \begin{pmatrix} 0.823300 & 0.547975 & -0.122396 + i0.083181 \\ -0.294674 + i0.051493 & 0.607002 + i0.034273 & 0.735451 \\ 0.480155 + i0.046295 & -0.573713 + i0.030813 & 0.661219 \end{pmatrix}, \quad (\text{C6})$$

with the slight differences (within uncertainties) resulting from $\sin^2\langle\theta\rangle \neq \langle\sin^2\theta\rangle$.

Appendix D: Computing the Magic Power of a Unitary Operator

The magic power of a unitary operator $\hat{\mathbf{S}}$, denoted by $\overline{\mathcal{M}}(\hat{\mathbf{S}})$, is defined to be the average magic induced by the operator on all n -qudit stabilizer states $|\Phi_i\rangle$:

$$\overline{\mathcal{M}}(\hat{\mathbf{S}}) \equiv \frac{1}{\mathcal{N}_{ss}} \sum_{i=1}^{\mathcal{N}_{ss}} \mathcal{M}(\hat{\mathbf{S}}|\Phi_i), \quad (\text{D1})$$

where \mathcal{N}_{ss} denotes the total number of n -qudit stabilizer states. \mathcal{M} is a measure of magic, which we define in terms of SREs in Eq. (B5).

1. The Magic Power of the Single-Neutrino Evolution Operator

The magic power of the free-space single neutrino evolution operator is computed using Eq. (D1). For two flavors, it is found to be

$$\overline{\mathcal{M}}_2(\hat{U}) = 2 \left[1 - \frac{1}{3} \log_2 \left(7 + \cos \left(\frac{2\delta m_{21}^2 t}{E} \right) \right) \right], \quad (\text{D2})$$

and for three flavors

$$\overline{\mathcal{M}}_2(\hat{U}) = -\frac{3}{4} \log_2 \left[\frac{1}{81} \left(57 + 8 \cos \left(\frac{3\delta m_{21}^2 t}{E} \right) + 8 \cos \left(\frac{3\Delta m_{31}^2 t}{E} \right) + 8 \cos \left(\frac{3(\Delta m_{31}^2 - \delta m_{21}^2) t}{E} \right) \right) \right]. \quad (\text{D3})$$

Appendix E: Tables of Results

In this section, we provide tables of results displayed in figures in the main text.

Appendix F: The Evolution of Select Quantities

To illustrate the general behavior of the evolution of three-flavor neutrino systems, we present results for the probabilities, \mathcal{M}_2 , concurrence, generalized-concurrence, the 2-tangle and 4-tangle, in systems resulting from initial states of $|\nu_e\rangle^{\otimes 5}$ and, as an example of mixed-flavor state, $|\nu_e\nu_e\nu_e\nu_\mu\nu_\tau\rangle$.

The probabilities are found from projections of each of the neutrinos onto the mass eigenstates as a function of time. For a system of N_ν neutrinos, this gives rise to $3N_\nu$ curves evolving from just three values at the initial time. The concurrence and generalized-concurrence are found by forming the single-neutrino reduced-density matrix for

N_ν	Method	Asymp. \mathcal{M}_2 for $ \nu_e\rangle^{\otimes N_\nu}$	Asymp. \mathcal{M}_2 for $ \nu_e\rangle, \nu_\mu\rangle, \nu_\tau\rangle$
2	Trotterized, $\Delta\kappa t = 0.05$	0.755(19)	0.97(5) ($e\mu$) 0.96(4) ($e\tau$)
2	Numerical ODE solution	0.755(19)	0.97(4) ($e\mu$) 0.97(3) ($e\tau$)
3	Trotterized, $\Delta\kappa t = 0.05$	0.694(10)	1.06(2) ($e\mu\tau$)
3	Numerical ODE solution	0.695(10)	1.06(2) ($e\mu\tau$)
4	Trotterized, $\Delta\kappa t = 0.05$	0.637(5)	1.125(7) ($e\mu\mu\tau$) 1.139(8) ($e\mu\tau\tau$)
4	Numerical ODE solution	0.638(5)	1.120(8) ($e\mu\mu\tau$) 1.140(9) ($e\mu\tau\tau$)
5	Trotterized, $\Delta\kappa t = 0.05$	0.589(3)	1.133(6) ($ee\mu\mu\tau$) 1.154(3) ($ee\mu\tau\tau$) 1.243(2) ($\tau\mu e\tau\mu$)
6	Trotterized, $\Delta\kappa t = 0.05$	0.548(2)	1.117(4) ($\tau\tau\mu\mu e e$) 1.182(2) ($ee\mu\tau\tau\tau$) 1.192(2) ($e\mu\mu\tau\tau\tau$) 1.236(2) ($\tau\mu\tau\mu\tau e$) 1.265(1) ($e\mu\tau e\mu\tau$) 1.280(1) ($\mu\tau e\mu\tau\mu$) 1.292(1) ($\tau\mu e\tau\mu\tau$)
7	Trotterized, $\Delta\kappa t = 0.05$	0.516(2)	0.6608(54) ($\tau e e e e e e$) 1.1309(8) ($ee\mu\mu e e\tau$) 1.2285(6) ($\tau\tau\mu\mu e e\tau$) 1.2522(6) ($\tau\tau\tau\tau\tau\tau$) 1.2694(13) ($e\mu\tau e\mu\tau e$) 1.2945(6) ($e\mu\tau e\mu\tau\tau$) 1.3072(3) ($\tau\tau e\tau\tau\tau\tau$) 1.3163(3) ($\tau\mu e\tau e\tau\mu$) 1.3190(4) ($\tau\mu e\tau\mu e\tau$) 1.3243(2) ($\tau\mu e\tau\mu\tau\mu$)
8	Trotterized, $\Delta\kappa t = 0.05$	0.488(1)	1.1591(5) ($\tau\tau e e\tau\tau e e$) 1.161(1) ($eee\mu\mu\tau\tau\tau$) 1.1693(5) ($\tau\tau\tau\mu\mu\mu e e$) 1.2293(3) ($e e\tau\tau e e\tau\tau$) 1.2433(3) ($\mu\mu\tau\tau e e\tau\tau$) 1.270(2) ($\tau e\tau e\tau e\tau e$) 1.3292(2) ($e\mu\tau e\mu\tau e\mu$) 1.3460(1) ($\tau\mu e\tau\mu\tau\mu\tau$) 1.35126(7) ($\tau\mu e\tau\mu e\tau\mu$)

TABLE I. The asymptotic magic per neutrino for select initial states, as displayed in Fig. 4 of the main text. The third and fourth column headers denote the flavor composition of the initial states, i.e., either all electron-type, or a mix of all three flavors. The ‘‘Numerical ODE solutions’’ were performed using 9th order lazy and 4th order stiffness-aware interpolation and Tolerances: 10^{-8} absolute, 10^{-8} relative.

each neutrino in the state, $\hat{\rho}_i$, and computing its eigenvalues, $\lambda_{i1,i2,i3}$. The concurrence for each $\hat{\rho}_i$ is determined by four times the sum of products of two eigenvalues, while the generalized-concurrence is the product of the three eigenvalues. These are then summed over each of the neutrinos, i.e.,

$$C = 4 \sum_i (\lambda_{i1}\lambda_{i2} + \lambda_{i1}\lambda_{i3} + \lambda_{i2}\lambda_{i3}) \quad , \quad G = \sum_i \lambda_{i1}\lambda_{i2}\lambda_{i3} \quad . \quad (\text{F1})$$

The n -tangles are formed from matrix elements of n insertions of the SO(3) generators [109], \hat{J}_i^n , where,

$$J_1 = \begin{pmatrix} 0 & 0 & 0 \\ 0 & 0 & -i \\ 0 & i & 0 \end{pmatrix} \quad , \quad J_2 = \begin{pmatrix} 0 & 0 & i \\ 0 & 0 & 0 \\ -i & 0 & 0 \end{pmatrix} \quad J_3 = \begin{pmatrix} 0 & -i & 0 \\ i & 0 & 0 \\ 0 & 0 & 0 \end{pmatrix} \quad , \quad (\text{F2})$$

and averaging over the squared-magnitude, i.e.,

$$\tau_4 = \frac{1}{\mathcal{N}_4} \sum_i \sum_{a \neq b \neq c \neq d} |\langle \psi | \hat{J}_{i,a} \hat{J}_{i,b} \hat{J}_{i,c} \hat{J}_{i,d} | \psi \rangle|^2 \quad , \quad (\text{F3})$$

where \mathcal{N}_4 is the number of contributions to the sum. This is the generalization of the n -tangles for two-flavor systems.

1. Initially $|\nu_e\rangle^{\otimes 5}$

Figure 5 displays the probabilities of being in one of the three mass eigenstates and the magic as a function of time starting from an initial state of $|\nu_e\rangle^{\otimes 5}$, while Fig. 6 displays the concurrence, generalized-concurrence, τ_2 and τ_4 . It can

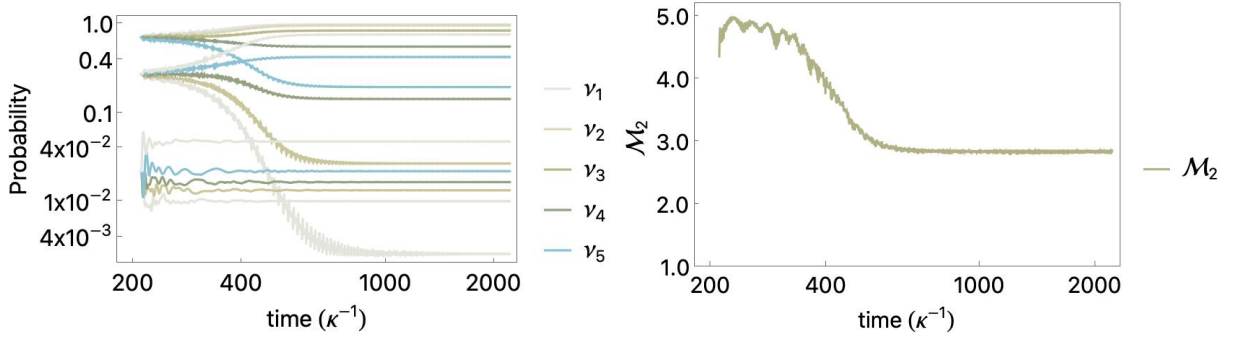


FIG. 5. The left panel shows the probabilities of neutrinos initially in the $|\nu_e\rangle^{\otimes 5}$ state evolving into one of the three mass eigenstates, while the right panel shows the evolution of the magic \mathcal{M}_2 .

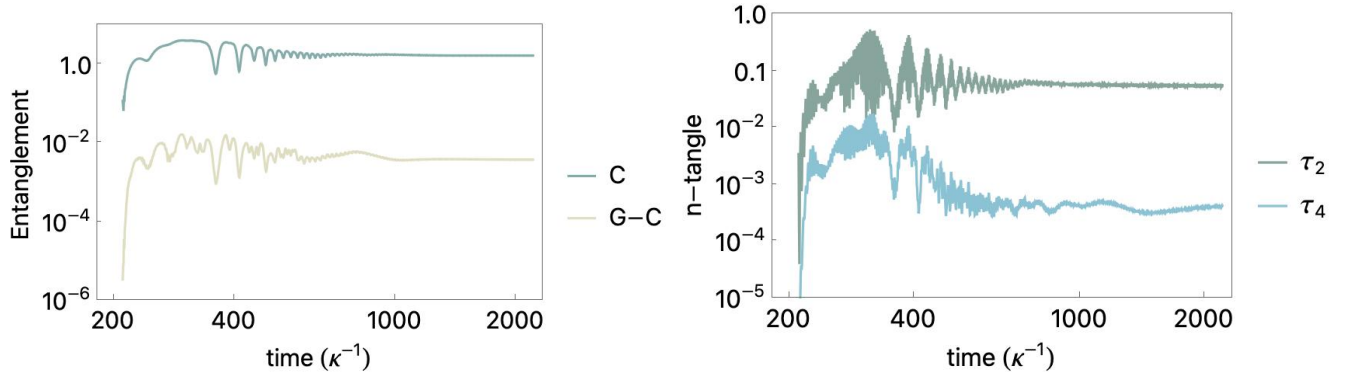


FIG. 6. The left panel shows the sum of the concurrence (C) and generalized-concurrence (G-C) of neutrinos initially in the $|\nu_e\rangle^{\otimes 5}$ state evolving into the three mass eigenstates, while the right panel shows the evolution of the 2-tangle τ_2 and 4-tangle τ_4 .

be observed that while the eigenstate projections and magic appear to approach asymptotic values, the concurrences and n -tangles approach appears to be somewhat delayed.

2. Initially $|\nu_e\nu_e\nu_\mu\nu_\mu\nu_\tau\rangle$

Here we display the corresponding results for an initial state of $|\nu_e\nu_e\nu_\mu\nu_\mu\nu_\tau\rangle$. The probability of being in a mass

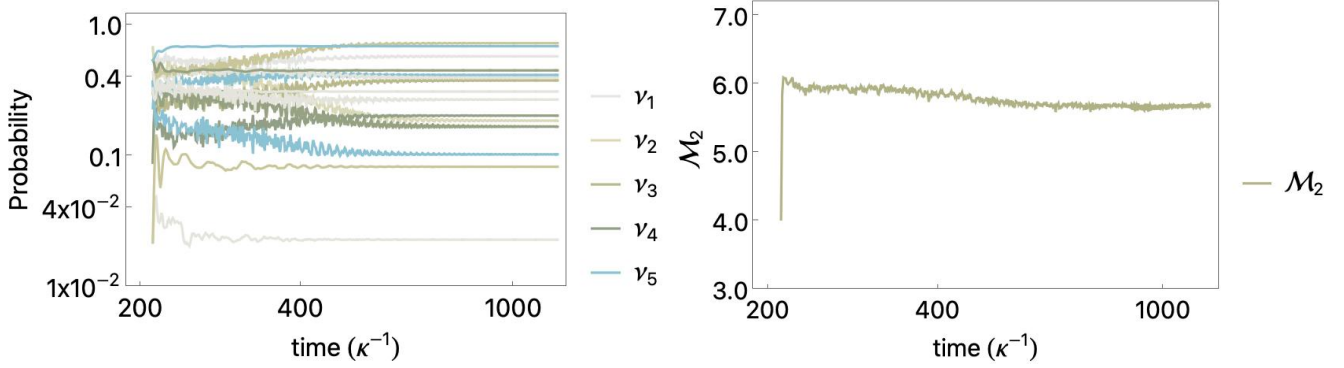


FIG. 7. The left panel shows the probabilities of neutrinos initially in the $|\nu_e\nu_e\nu_\mu\nu_\mu\nu_\tau\rangle$ state evolving into one of the three mass eigenstates, while the right panel shows the evolution of the magic \mathcal{M}_2 . The results were generated with a Trotter time interval of $\kappa\Delta t = 0.05$, and sampled every 20 time steps for display purposes.

eigenstate exhibits quite different behavior when compared with a $|\nu_e\rangle^{\otimes 5}$ initial state, as shown in Fig. 7. This is also the case for \mathcal{M}_2 , which rapidly rises to its maximum value and stays approximately near this value throughout the evolution. The value of $\mathcal{M}_2 \sim 6$ is noticeably larger than the maximum magic that a tensor-product state of $N_\nu = 5$ can support, and thus the two-neutrino interactions are generating magic in the multi-neutrino systems. As shown in

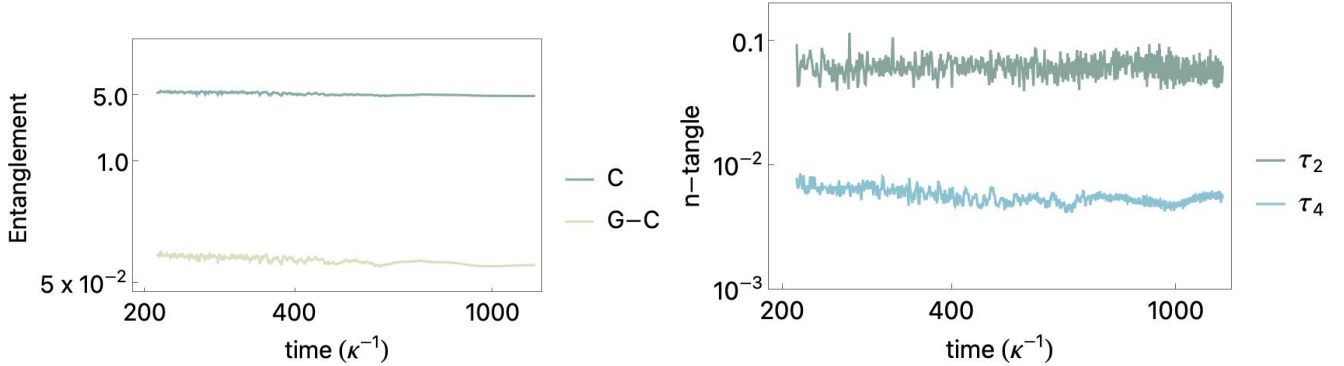


FIG. 8. The left panel shows the sum of the concurrence (C) and generalized-concurrence (G-C) of neutrinos initially in the $|\nu_e\nu_e\nu_\mu\nu_\mu\nu_\tau\rangle$ state evolving into the three mass eigenstates, while the right panel shows the evolution of the 2-tangle τ_2 and 4-tangle τ_4 . The results were generated with a Trotter time interval of $\kappa\Delta t = 0.05$, and sampled every 20 time steps for display purposes.

Fig. 8, the concurrence and generalized-concurrence exhibit a similar behavior and have values that are substantially larger than for the $|\nu_e\rangle^{\otimes 5}$ initial state. While τ_2 behaves differently with time, its asymptotic value is similar. In contrast, τ_4 is substantially larger asymptotically.